Materials Research Proceedings 28 (2023) 293-304 https://doi.org/10.21741/9781644902479-32

In-plane deformation measurements for validation of composite forming simulations

BRANDS Dennis[1,2,a,*], VAN KAMMEN Kevin M.[1,b], WIJSKAMP Sebastiaan[2,c], GROUVE Wouter J.B.[1,d] and AKKERMAN Remko[1,2,e]

[1]Faculty of Engineering Technology, Chair of Production Technology, University of Twente, Enschede, the Netherlands

[2]ThermoPlastic composites Research Center (TPRC), Enschede, the Netherlands

[a]d.brands@utwente.nl, [b]k.m.vankammen@student.utwente.nl, [c]sebastiaan.wijskamp@tprc.nl, [d]w.j.b.grouve@utwente.nl, [e]r.akkerman@utwente.nl

Keywords: Composite Forming, Thermoplastic, Unidirectional, Carbon Fiber, Photogrammetry, Validation

Abstract. Validation of composites forming simulations is essential to improve simulation predictions. Detailed validation requires reliable and well-controlled forming processes with precise methods for comparison to simulation results. This study presents some preliminary results from press forming experiments with cross-ply laminates shaped over a dome geometry. The material studied is a unidirectional carbon-fiber reinforced thermoplastic composite. The forming experiments were combined with a deformation measurement technique based on photogrammetry to measure the in-plane deformation on the surface of the laminate after forming. The obtained full-field deformation measurements allow for a direct and quantitative comparison with simulations. The accuracy and precision of the methodology are discussed in detail. The combination of a versatile forming experiment and a detailed analysis method as presented in this article could enable a more precise validation of composite forming simulations.

Introduction

The development of composite forming simulation models based on finite elements has already resulted in various commercial implementations to date. [1] These high-fidelity design tools can be used to address challenges in the complex relation between part design, process design and the occurrence of defects through the prediction of deformation and stress during processing. In this way, virtual design iterations using simulations allow engineers to mitigate some of the risks associated with production delays, unforeseen costs and wasted material.

However, like any model, composite forming simulations will have inherent limitations in terms of accuracy and precision. Moreover, because simulations are generally an ideal representation of reality, they cannot always account for material variability or uncertainties in boundary conditions. The prediction of wrinkling is a particular challenge in composites forming, because these defects can be relatively small compared to the overall geometry and the physical buckling phenomenon underlying this defect is sensitive to the aforementioned variabilities and uncertainties. Therefore, validation efforts are required to evaluate the limitations of current simulation models. Knowing the discrepancies properly can serve as a basis for future improvements to composites forming simulations.

This article follows up a previous publication [2] where a dome was used to study wrinkling with changing laminate geometry and layup on a simple generic toolset. Wrinkles were observed more easily by not closing the press fully and careful choice of the boundary conditions allowed the material behavior to dominate over handling influences in the result. Those results already taught a lot about the material's limitation in forming. However, for validation, the wrinkling can

mainly be used as a qualitative measure, limiting the accuracy due to subjective interpretation. Wrinkling quantification may be possible through measurement of the laminate surface and an appropriate wrinkling metric, such as local curvature as featured in the work of Dörr et al. [3] Nevertheless, a quantitative comparison of wrinkles may still be complicated due to the variability in exact shape, size and location of individual wrinkles and folds. Hence, despite wrinkling being the predominant defect of interest, it only allows for an indirect way to validate many of the complex inputs (e.g. material models) to the simulation.

In a related field of study, sheet metal forming, a well-established technique to validate simulations is the measurement of the deformations. Hence, professionalized and automated implementations of such systems, for example the ARGUS system by GOM Metrology [4], could serve as a source of inspiration to further develop high-end techniques applicable to composites forming. For metal forming, typically, a polka-dot pattern with a 1-5 mm resolution is applied to the blank using direct printing or chemical etching. The deformed pattern after forming is digitized using photogrammetry and used to calculate major strain, minor strain and thickness reduction. These quantities may be compared against simulations directly or related to forming defects through a forming limit diagram.

In composites forming the main deformation of interest is arguably the reorientation of the fiber direction(s), or the related shear angle [5]. Limited extensibility in fiber direction will have a pronounced effect on the overall deformation, resulting in dominant shear behavior and local thickening rather than thinning. The fiber directions may be tracked intuitively using drawn lines [6], a tracer in the fabric [7,8] or directly from the materials' inherent pattern [9,10]. However, full field strain measurements, using photogrammetry for example, provide a more complete picture of the local deformations. Haanappel et al. [11] have applied photogrammetry on a dot pattern to measure the deformation from stamp forming thermoplastic composites, allowing correlation of the measured shear strains on the top surface with simulation results. Sachs et al. [12] extended this technique by applying a pattern on both sides of the laminate to measure the relative movement of the outer plies through the thickness direction, used to validate ply-ply slip and friction in the simulations. Kunze et al. [13] showed that photogrammetry can even be applied on internal plies of a layup through CT measurements and a pattern applied with a special paint for good x-ray contrast.

This article presents a study where the versatile dome forming experiment is combined with a deformation measurement technique based on photogrammetry. The resulting measured deformation fields enable a quantified means to directly validate the in-plane material behavior in composite forming simulation models. By varying the blank dimensions and layup, the dome experiment allows for a wide range of deformations, highlighting the influence of the various underlying deformation mechanisms. However, in this study the layup will be limited to cross-ply, because of the pronounced role in-plane shear deformation has during forming and the direct link with wrinkling defects through the other dominant deformation mechanism, namely bending.

On a historical side note, there is a striking resemblance between the study described in this article and the work by Martin et al. [14] published 30 years ago. However, the capabilities of modern day computer simulations require a more detailed and quantified look into the local deformations, making this topic ever more relevant today.

Method

In preparation for the forming experiments, flat laminates were prepared from Toray TC1225 and Solvay APC materials, both are unidirectional carbon fiber reinforced thermoplastic composite tapes typically applied in the aerospace industry. Some datasheet characteristics on these materials are collected in Table 1.

Materials Research Proceedings 28 (2023) 293-304 https://doi.org/10.21741/9781644902479-32

Table 1. Material characteristics, from datasheet [15,16].

	Toray TC1225	Solvay APC
Fiber	T700	AS4D
Fiber areal weight [g/m2]	145	145
Fiber volume fraction [%]	59	59
Matrix	LM-PAEK	PEKK-FC
Resin content by weight [%]	34	34
Glass transition temperature [°C]	147	159
Melting temperature [°C]	305	337
Consolidated ply thickness [mm]	0.14	0.14

Laminates were press consolidated from loosely stacked plies inside a picture frame mold, with multiple laminates separated by caul sheets and release agents applied to all tooling surfaces. Solvay APC was consolidated at 375°C, 10 bar for 15 minutes and Toray TC1225 at 365°C, 10 bar for 20 minutes. Finally, blanks were cut to final dimension using a water cooled diamond saw. Blanks were dried at 120°C overnight and press formed the same day. The test matrix for the forming experiments is comprised of different layups and blank dimensions according to Table 2.

Table 2. Test matrix with number of formed blanks for combinations of width and layup. The same test matrix was used for both materials.

		$[0/90]_{2s}$	$[45/-45]_{2s}$	$[90/0]_{2s}$	$[0/90]_{4s}$
Width	40 mm	2			2
	80 mm	2			2
	110 mm	2			2
	140 mm	4	2	2	2

# Plies	8	16
Length	295 mm	380 mm
Thickness	≈ 1.1 mm	≈ 2.2 mm
Tool gap	3.1 mm	4.2 mm

Prior to forming, a dot pattern was applied in a rectangular grid to all blanks, see Fig. 2a. Dots are spaced 5 mm apart with a 1.7 mm diameter and the grid is aligned with both fiber directions in the layup. The pattern is painted onto the laminate using a heat resistant silver spray paint and a mask in the form of a sticker. This mask was cut using a CNC-plotter and applied to the laminate using transfer tape to prevent deformation.

Press forming was conducted on the 200 ton Pinette Emidecau Industries press at TPRC, in which the same procedure was applied as previous research [2]. Steel tooling was used having a square base and a hemisphere dome shaped cavity, with dimensions according to Fig. 1. The 8-ply laminates use a 1.1 mm nominal cavity, where it is 2.2 mm for all 16-ply laminates. The tool temperature was 220°C for all experiments.

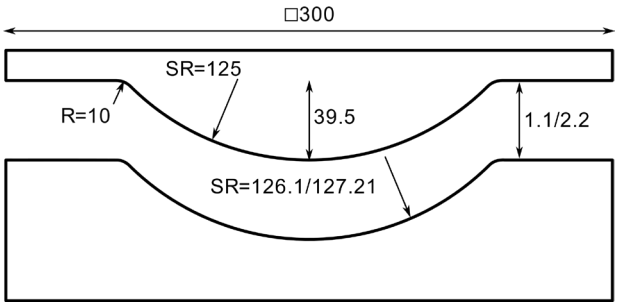

Fig. 1. Hemisphere tool set illustration with dimensions in millimeters. A single male punch is used in combination with two female dies for specific nominal cavity sizes.

The forming process cycle consists of suspending the blank in a shuttle frame, equal to the previous study [2], with the dot pattern facing downwards towards the female die tooling. The blank was then heated to 365°C for Toray TC1225 or 375°C for Solvay APC inside an infrared oven, before a quick automatic transfer places it between the press tooling, which close to form the part. The velocity of the tool is approximately 100 mm/s initially and switches to 20 mm/s when the tools are spaced 10 mm apart. No consolidation pressure was applied, instead a fixed tool gap was used according to Table 2.

The deformation measurement method and calculation is similar to the study of Haanappel et al. [11], which utilizes photogrammetry to digitize the dot pattern on formed parts. First, the part is photographed in a dedicated photography set-up with adequate lighting, a remote control turntable, a surface with reference marks and polarizing light filters to cancel out unwanted specular reflections. A Sony DSC-RX100M3 digital camera was used with a small aperture (f/8) and a low iso-number (200) for a large depth of field and high picture quality. Each part was photographed from 16 equidistant angles around the part, at a fixed elevation. An example photo is shown in Fig. 2b.

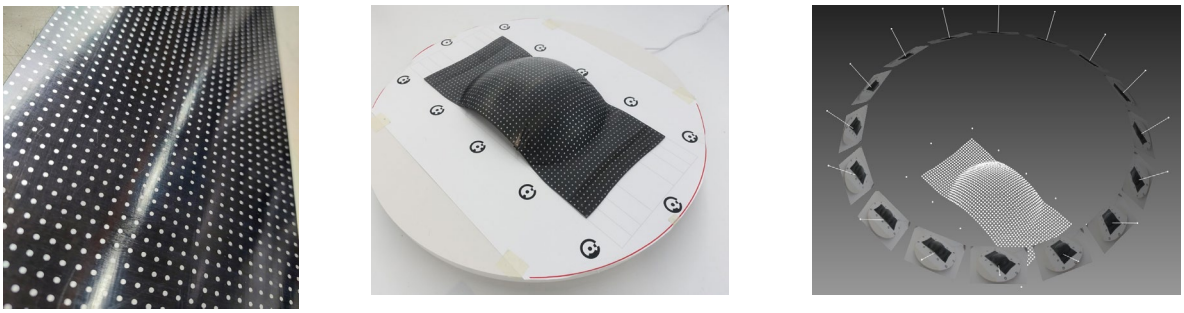

(a) (b) (c)

Fig. 2. (a) Dot pattern on undeformed laminate (b) Formed Solvay APC $[0/90]_{2s}$ 140 mm wide part in photography setup (c) Digitized dot pattern in the PhotoModeler [17] software with camera positions for individual photos.

These photos were subsequently analyzed in the photogrammetry software PhotoModeler [17] First, all visible dots are marked for each photo. Then, the software optimizes for the camera orientation and parameters to determine the locations of each dot in 3D space, including a confidence region. A reference length is used to scale the point cloud to real world length units. An example of a final PhotoModeler project state is shown in Fig. 2c. The undeformed configuration was not analyzed with photogrammetry, but assumed to match the design of the paint mask pattern. Finally, points are sorted to have corresponding node locations and meshed with a triangular element topology that is the same for both configurations.

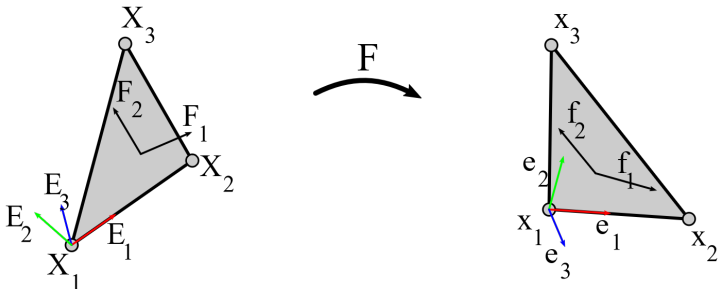

Fig. 3. Vector definitions in initial (left) and deformed (right) configurations.

The deformation can now be calculated for each triangular element by comparing the deformed configuration with the initial configuration, see Fig. 3. Elements in the initial configuration are defined by three nodes in 3D space (X_1, X_2, X_3), linear shape functions, two fiber directions (F_1, F_2) and a local coordinate system. The deformed configuration is similar, but has unknown fiber directions still. The deformation gradient tensor $\boldsymbol{F}$ is readily calculated from the shape functions [18] based on the 2D nodal coordinates in their respective local coordinate systems.

The deformation gradient tensor maps the fiber directions to the deformed configuration using

$$f_1 = \boldsymbol{F} \cdot F_1 \quad \text{and} \quad f_2 = \boldsymbol{F} \cdot F_2 \,. \tag{1}$$

And, based on the difference in fiber directions between configurations, the shear angle is calculated using

$$\gamma = \cos^{-1}(f_1 \cdot f_2) - \cos^{-1}(F_1 \cdot F_2), \tag{2}$$

based on unit fiber directions. Although only a single fiber direction is present on the outer ply, it is assumed that the second fiber direction on the ply below behaves according to the same deformation gradient. The latter term in equation 2, the initial fiber angle, is 90° for all laminates considered in this article. Next, the Green-Lagrange strain can be calculated from the deformation gradient according to

$$\boldsymbol{E} = {}^{1}/_{2}\,(\boldsymbol{F}^T \cdot \boldsymbol{F} - \boldsymbol{I})\,, \tag{3}$$

where $\boldsymbol{I}$ is the second order identity tensor. Standard tensor coordinate transformation rules are applied to align it with the first fiber direction. Finally, results calculated for each element are averaged component wise in the nodes for continuity arguments.

Results

Only six parts in Solvay APC material were analyzed for in-plane deformation due to an identified issue, which will be addressed in the discussion section. Pictures for each of the formed parts are nevertheless included in the digital dataset that is published alongside this article.

Fig. 4 shows the obtained results for a Solvay APC $[0/90]_{2s}$ dome with a width of 140 mm. Three components of the Green-Lagrange strain show that the majority of the deformation occurs in shear (xy-component). Most shear deformation is located in the four corners, near the base of the hemisphere, with a 10-13° shear angle at maximum. The shear deformation is not exactly symmetric over the vertical axis because the laminate was not centered over the dome geometry.

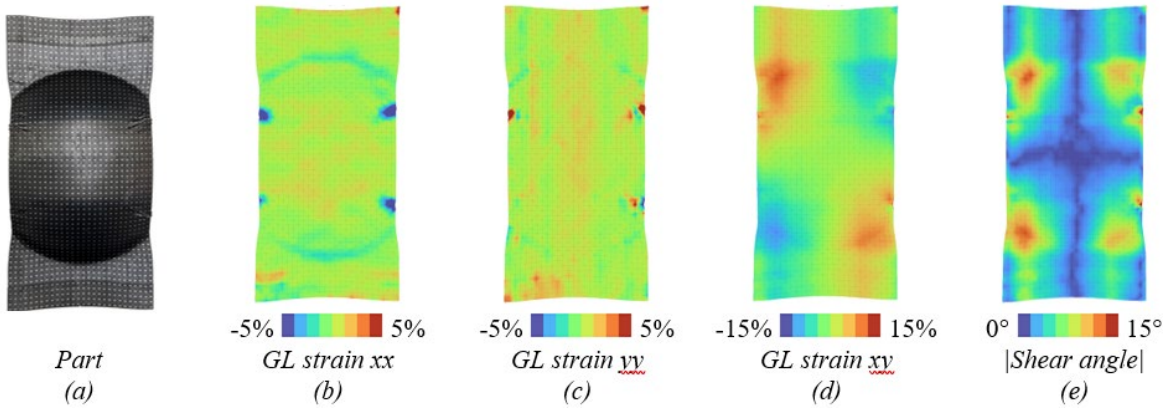

Fig. 4. Deformation results for a Solvay APC $[0/90]_{2s}$ dome 140 mm wide. The xx-direction is based on the local fiber direction, originally in length direction of the laminate.

Four distinct areas with significant compressive normal strain in xx-direction (fiber direction) are observed, which correspond with the locations of the wrinkles on the formed part. In the vicinity of a wrinkle the material is concentrated, bringing points closer together, therefore showing a compressive strain. The transverse strain (yy-component) has a band of positive strain values running in length direction over the dome, which could be related to transverse flow deformation. Near the wrinkles the distorted elements result in local high and low values for the transverse strain.

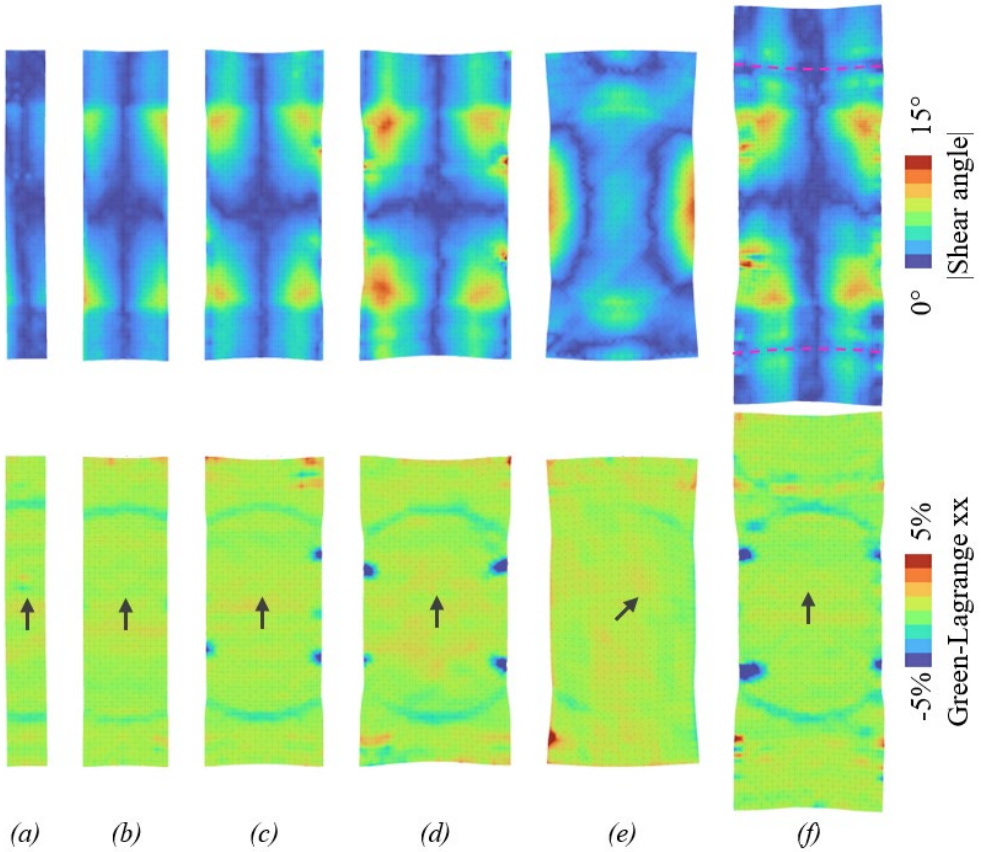

Fig. 5. Results for six domes from Solvay APC. Above: Absolute shear angle. Below: Strain in fiber direction (approximately indicated using an arrow). (a) $[0/90]_{2s}$ 40mm (b) $[0/90]_{2s}$ 80mm (c) $[0/90]_{2s}$ 110mm (d) $[0/90]_{2s}$ 140mm (e) $[45/-45]_{2s}$ 140mm (f) $[0/90]_{4s}$ 140mm.

Fig. 5 shows the most relevant results for each of the six parts analyzed. Subfigures (a)-(d) show parts with the same $[0/90]_{2s}$ layup and a varying width. It is observed that the shear deformation increases with width and the deformation is propagated more from the base of the dome towards the edge of the laminate. However, for the 110 mm and 140 mm wide parts the shear deformation is close to zero on the far left and right edge below the dome, indicating a sudden drop in in-plane deformation. This finding corresponds with the observations for the Green-Lagrange xx results in Fig. 5a-d, where wrinkling is indicated for widths of 110 and 140 mm by compressive strain. The results obtained for these parts thereby illustrate the interrelation between in-plane deformations, in particular the presence of local wrinkling, and the resulting decrease in shear deformation elsewhere in the part.

The part with a $[45/-45]_{2s}$ layup in Fig. 5e shows a completely different shear deformation pattern and no compressive strain in fiber direction. Indeed, no wrinkling was observed on this part. Therefore, this is possibly an interesting validation case for simulations due to the reduced influence of bending whilst still introducing large shear deformation.

The part with a $[0/90]_{4s}$ layup in Fig. 5f has the same typical shear deformation pattern in the four corners as the 8-ply variant, however, less shear deformation is propagated from the base of the hemisphere to the part edge, which may be related to the longer laminate length. Also, some deformation is concentrated around the two PI-tapes that were used to handle the molten laminate throughout the press forming process, indicated with magenta lines in Fig. 5f. This means that the influence of the tape cannot be neglected for this forming process, possibly due to adhesion and friction with the laminate, or an effect on the local laminate temperature.

Discussion

Because of the goal to use these deformation measurements for accurate validation of forming simulations, the discussion in this article focusses on the several aspects concerning the accuracy and precision of the methodology and its results.

Fig. 6 shows the element values for absolute shear angle. The element value is an intermediate result in the calculation, right before the nodal averaging is applied to obtain Fig. 5. For some parts, a pattern of lines is observed in these element value, possibly indicating an accuracy issue. Interestingly, this pattern cancels out during the nodal averaging step in the calculation, hence they are not observed in Fig. 5. Moreover, it seems that not all parts suffer equally from this artifact, meaning it is an inconsistent error in a fixed methodology.

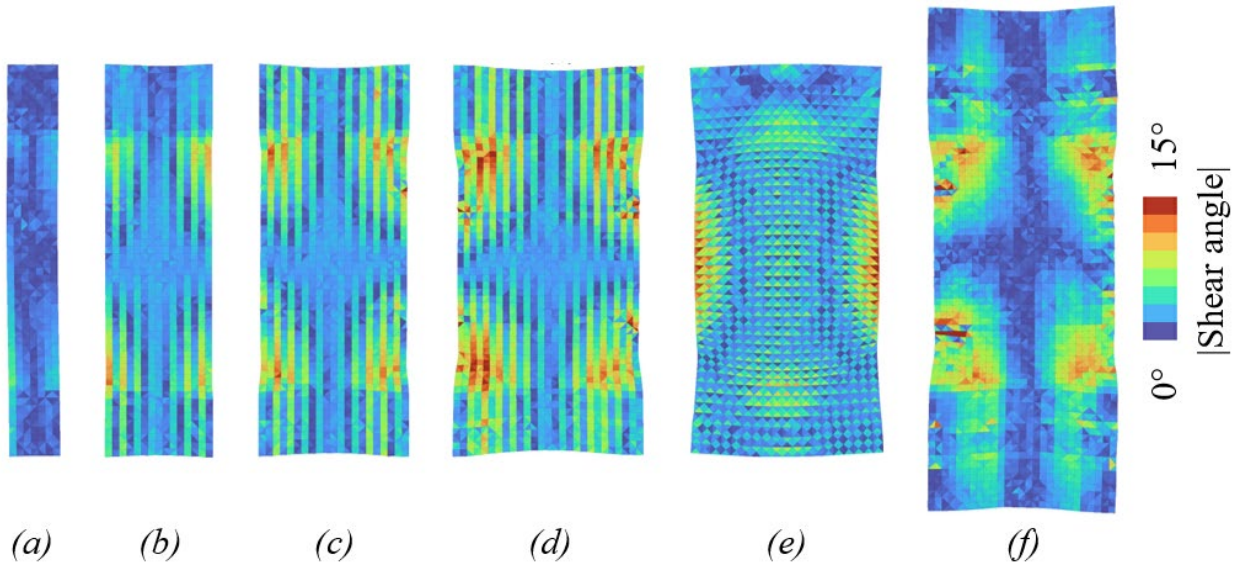

Fig. 6. Element values of the absolute shear angle. Subfigures a-f correspond with Fig. 5, in which the nodal values are plotted.

The cause for the observed element value artifacts was found in the application method of the dotted pattern onto the undeformed laminates. Fig. 7 shows a zoomed photo of an undeformed laminate, where alternating rows of dots are shifted horizontally. The same issue was found for the pattern in the paint mask sticker. Possibly, the scanning strategy of the plotter introduced this relatively repeatable error. The shift was quantified to be approximately 0.2 mm from a leftover sticker.

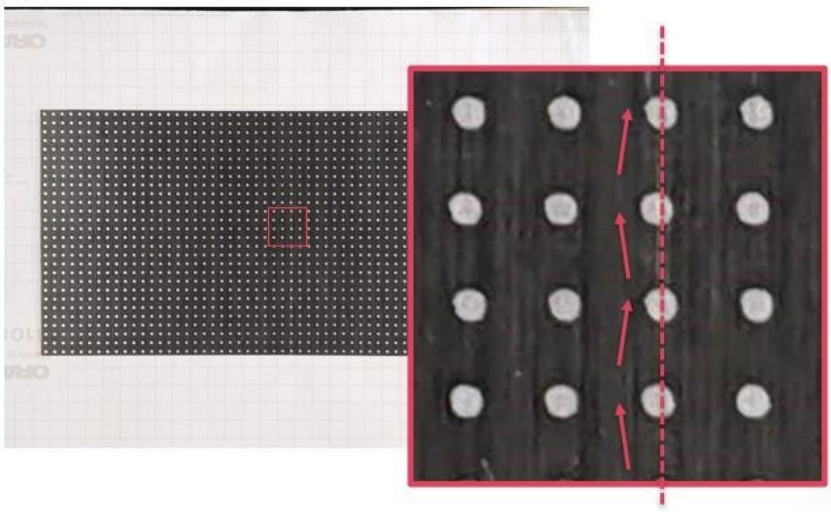

Fig. 7. Zoomed area of an undeformed laminate. A distortion is observed in the dot pattern where every other row has a horizontal shift.

Due to the repetitive nature of the error, a correction was attempted by manually assigning a 0.2 mm displacement to every other row of nodes in the undeformed configuration. This technique allows to resolve the striped patterns in the element values observed in Fig. 6c and 6d. The parts in Fig. 6a and 6f don't seem to have any issues, therefore not requiring any correction. Finally, parts in Fig. 6b and 6e have an inhomogeneous error and correction only works successfully for some areas. The effect on the nodal values is mostly zero, since alternating plus and minus contributions are averaged to zero in central node locations. However, non-zero contributions

remain in the nodal values on the edges of the part. The magnitude of which can be understood geometrically from the angle formed by the distortion and the grid size, through $\Delta\gamma = \left(\frac{0.2}{5}\right) \approx 2.3°$. Hence, it may be concluded that the inaccurate placement of the pattern resulted in a significant loss of accuracy for the nodal values on the edge of the part. Moreover, because the error can be inhomogeneous and inconsistent between parts, it is impossible to truly correct for.

The precision of the photogrammetry technique used to measure the locations of the dots in the deformed configuration will inevitably lead to a precision for the in-plane deformations measured. The PhotoModeler software [17] output includes precision values on the x-, y- and z-coordinates for each node, specified as one standard deviation for a normal distribution. This probability can be propagated using Monte Carlo simulation to assess its influence on the nodal values for each of the in-plane deformation results.

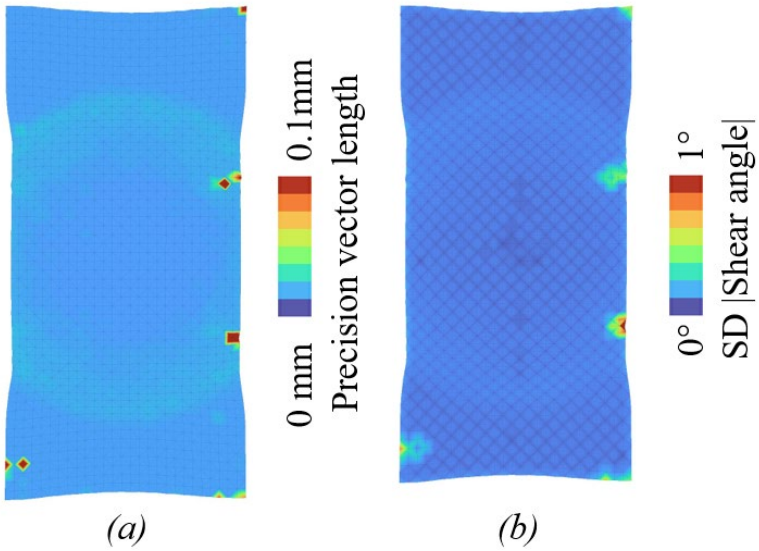

Fig. 8. Solvay APC $[0/90]_{2s}$ 140mm wide. (a) Euclidean length of the precision vector (standard deviations on x- y- and z-positions) (b) Standard deviation on the nodal absolute shear angle, obtained using Monte Carlo simulation from the precision on node positions.

An example is shown in Fig. 8 for the 140 mm wide $[0/90]_{2s}$ part in Solvay APC. The precision on the nodal positions, resulting from the photogrammetry analysis, is shown in Fig. 8a. It is observed that the majority of points was determined with a standard deviation of about 0.015mm on its 3D position, with a few outliers. Subsequently, a thousand meshes in the deformed configuration were sampled, with each node position based on individual normal distributions in x-, y- and z-direction. The resulting in-plane deformation values are approximately normally distributed with a standard deviation indicative of the precision, see Fig. 8b. Instinctively, a large precision vector results in higher standard deviation on the deformation in the surrounding area. Besides a few outliers, the majority of points has a standard deviation less than 0.15° on the absolute shear angle and 0.15% on each of the Green Lagrange strain components. Naturally, these values will be affected by the details of the photogrammetry implementation and are therefore specific to this study.

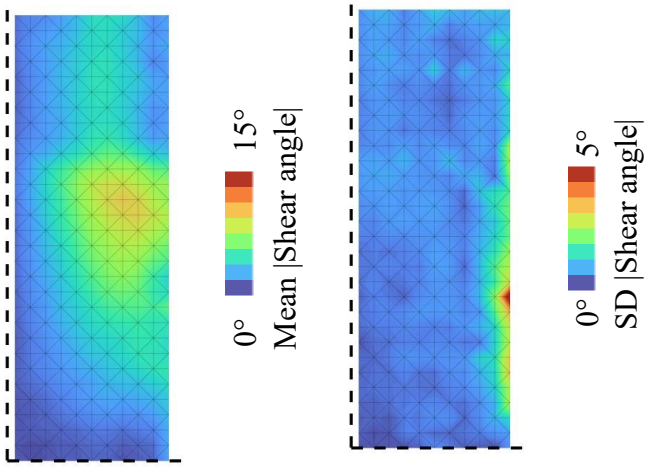

Fig. 9. Nodal results from quadrant averaging for Solvay APC [0/90]2s 110 mm wide. Dashed lines indicate symmetry planes. Results plotted on undeformed geometry. (a) Mean value (b) Standard deviation.

Process variability is another important aspect to consider in validation studies. Although not directly obtained from the analyzed parts in this study, the expected symmetry in the forming results may be used to estimate this variability. Fig. 9 shows an example were the symmetries were used to average the absolute shear angle over each of the four quadrants. In this way, a more reliable mean deformation was obtained to compare against simulations. The spread is indicated by the standard deviation, which is higher than the precision achieved with the photogrammetry method. Nevertheless, it is recommended for future studies to analyze repetitive experiments to account for inherent process variability.

Summary

This article presented results from a forming study on cross-ply laminates from unidirectional thermoplastic composite material combined with measurements of the in-plane deformations. This proposed combination of methodologies is able to provide high-resolution strain and shear angle data, allowing a quantitative validation of composite forming simulations. It is particularly suited to investigate the delicate balance between the in-plane shear and bending (wrinkling) mechanisms that dominate the forming of cross-ply layups, which can be influenced experimentally by changing the width and layup of the laminate formed over the dome geometry.

Validating and improving forming simulations requires the most accurate and precise knowledge of the real-world process as possible. To this extent, the accuracy and precision of the deformation measurement technique have been discussed. An accuracy concern was raised related to the undeformed dot pattern in the current study, which affected the nodal results on edges of a part. However, this mistake can easily be overcome in the future. Furthermore, propagation of the precision in photogrammetry towards the in-plane deformation results using Monte Carlo simulation showed that, in this study, a standard deviation of 0.15° on the shear angle and 0.15% on the Green Lagrange strain values were achieved. As such, the repeatability of experiments may be the bottleneck to obtain reliable data for validating composite forming simulations accurately.

Data Availability

The dataset in this study is available in the 4TU.ResearchData repository under DOI: 10.4121/21688493

Acknowledgments

This work is part of the research program "MaterialenNL" with project number 17880, which is (partly) financed by the Dutch Research Council (NWO). The authors also gratefully acknowledge the financial and technical support from the industrial and academic members of the ThermoPlastic composites Research Center (TPRC).

References

[1] D. Dörr, W. Brymerski, S. Ropers, D. Leutz, T. Joppich, L. Kärger, F. Henning, A Benchmark Study of Finite Element Codes for Forming Simulation of Thermoplastic UD-Tapes, Procedia CIRP 66 (2017) 101–106. https://doi.org/10.1016/j.procir.2017.03.223

[2] D. Brands, L.G.Genova, E.R. Pierik, W.J.B. Grouve, S. Wijskamp, R. Akkerman, Formability Experiments for Unidirectional Thermoplastic Composites, Key Eng. Mater. 926 (2022) 1358–1371. https://doi.org/10.4028/p-x3g086

[3] D. Dörr, T. Joppich, F. Schirmaier, T. Mosthaf, L. Kärger, F. Henning, A method for validation of finite element forming simulation on basis of a pointwise comparison of distance and curvature, AIP Conf Proc 2016, 1769. https://doi.org/10.1063/1.4963567

[4] GOM Metrology, ARGUS: Optical forming analysis 2022. https://www.gom.com/en/products/3d-testing/argus (accessed December 7, 2022).

[5] A.C. Long, Composites forming technology, Woodhead Publishing Limited, 2007.

[6] P. de Luca, P. Lefébure, A.K. Pickett, Numerical and experimental investigation of some press forming parameters of two fibre reinforced thermoplastics: APC2-AS4 and PEI-CETEX, Compos. Part A Appl. Sci. Manuf. 29 (1998) 101–110. https://doi.org/10.1016/S1359-835X(97)00060-2

[7] C. Qian, R. Weare, C. Pasco, N. Kourra, A. Attridge, M. Williams, K. Kendall, Numerical and experimental studies of multi-ply woven carbon fibre prepreg forming process, Procedia Manuf. 47 (2020) 93–99. https://doi.org/10.1016/j.promfg.2020.04.142

[8] R.H.W. Thije, R. Akkerman, A multi-layer triangular membrane finite element for the forming simulation of laminated composites, Compos. Part A 40 (2009) 739–753. https://doi.org/10.1016/j.compositesa.2009.03.004

[9] Z. Wang, J. Luo, Z. Gong, Q. Luo, Q. Li, G. Sun, On correlation of stamping process with fiber angle variation and structural performance of thermoplastic composites, Compos. Part B Eng. 247 (2022) 110270. https://doi.org/10.1016/j.compositesb.2022.110270

[10] G. D'Emilia, A. Gaspari, E. Natale, Stamopoulos AG, Di Ilio A. Experimental and numerical analysis of the defects induced by the thermoforming process on woven textile thermoplastic composites. Eng. Fail. Anal. 135 (2022) 106093. https://doi.org/10.1016/j.engfailanal.2022.106093

[11] S.P. Haanappel, R.H.W. Thije, U. Sachs, B. Rietman, R. Akkerman, Formability analyses of uni-directional and textile reinforced thermoplastics, Compos. Part A 56 (2014) 80–92. https://doi.org/10.1016/j.compositesa.2013.09.009

[12] U. Sachs, S.P. Haanappel, B. Rietman, R. Ten Thije, R. Akkerman, Formability of fiber-reinforced thermoplastics in hot press forming process based on friction properties, Key Eng. Mater. 554-557 (2013) 501–506. https://doi.org/10.4028/www.scientific.net/KEM.554-557.501

[13] E. Kunze, B. Schwarz, T. Weber, M. Müller, R. Böhm, M. Gude, Forming Analysis of Internal Plies of Multi-Layer Unidirectional Textile Preforms using Projectional Radiography, Procedia Manuf. 47 (2020) 17–23. https://doi.org/10.1016/j.promfg.2020.04.110

[14] T.A. Martin, D. Bhattacharyya, R.B. Pipes, Deformation characteristics and formability of fibre-reinforced thermoplastic sheets, Compos. Manuf. 3 (1992) 165–172. https://doi.org/10.1016/0956-7143(92)90079-A
[15] Solvay. Solvay APC product datasheet 2021.
[16] Toray Cetex ® TC1225 product datasheet 2021.
[17] PhotoModeler Technologies. PhotoModeler Premium 2022. https://www.photomodeler.com/
[18] O.C. Zienkiewicz, R.L. Taylor, D.D. Fox, The Finite Element Method for Solid and Structural Mechanics, Seventh ed. Elsevier Ltd., 2014